RSC Advances

ROYAL SOCIETY OF CHEMISTRY

www.rsc.org/advances

RSC Advances

ARTICLE

$NiMoO_4$@$Co(OH)_2$ core/shell structure nanowire arrays supported on Ni foam for high-performance supercapacitors

Cite this: DOI: 10.1039/x0xx00000x

Received 00th 00 2014,
Accepted 00th 00 2014

DOI: 10.1039/x0xx00000x

www.rsc.org/

Weiji Ren,[ab] Di Guo,[a] Ming Zhuo,[a] Bingkun Guan,[a] Dan Zhang[c] and Qiuhong Li*[ab]

$NiMoO_4$@$Co(OH)_2$ core/shell structure nanowire arrays (NWAs) supported on Ni foam were successfully fabricated via a facile hydrothermal growth and electrochemical deposition route, applied in supercapacitors (SCs). The smart combination of $Co(OH)_2$ and $NiMoO_4$ nanostructures in nanowire arrays shows greatly enhanced electrochemical performance. The $Co(OH)_2$ nanoflakes wrapped on the surface of each $NiMoO_4$ nanowire uniformly, which could increase the capacitance of $NiMoO_4$ NWAs to a high areal capacitance of 2.335 F cm^{-2} at 5 mA cm^{-2} and 0.909 F cm^{-2} at 50 mA cm^{-2}, respectively. The electrode also exhibited good cycling ability, 83% of the initial capacity remained after 5000 cycles at a current density of 20 mA cm^{-2}. These results indicate that the $NiMoO_4$@$Co(OH)_2$ NWAs could be a promising electrode material for high-performance electrochemical capacitors.

1. Introduction

As one of the important electrochemical energy storage devices, supercapacitors (SCs) have attracted extensive research interest due to their excellent performance. Supercapacitors are superior with their high power density, fast recharge capability, and long cycle life.[1,2] As we know the excellent characteristics of supercapacitor benefit from the nanostructured electrode materials,[3] which have brought about great advancement of new supercapacitor technologies owing to their high surface area, short electron and ion transport pathways and so on.[4] In recent years, great efforts have been made to increase the capacitance and energy density of electrode materials. In this regard, many research groups have focused on the rational design of advanced core/shell heterostructures with fascinating synergetic properties.[5-15]

Pseudocapactive-type electrode materials, especially transition metal oxides[5-12] or hydroxides[9,26-34,37] such as ruthenium oxide (RuO_2), manganese oxide (MnO_2), nickel oxide (NiO) can provide high energy density relative to that delivered by electrical double layer capacitors using carbon-based active materials. Thus, transition metal oxides have been widely investigated as candidates for use in supercapacitors in view of their multiple oxidation states for pseudocapacitance generation. However, the experimentally obtainable capacitance values are often much lower than the theoretical expectations because of inadequate use of entire pseudocapacitive materials and limited electrical conductivity of metal oxides at high rate. To overcome above shortcomings, recently, metal molybdates such as $CoMoO_4$, $NiMoO_4$, $MnMoO_4$ have been demonstrated vastly to improve electrochemical performance over single component oxides. In particular, rate capability and durability have been significantly enhanced in nickel molybdate ($NiMoO_4$) supercapacitors,[16-25] with their high chemical stability and low cost.[18] For example, Liu et al.[19] demonstrated a $NiMoO_4 \cdot xH_2O$ nanorod supercapacitor with a maximum specific capacitance of 1136 F g^{-1} at 5 mA cm^{-2}. Till now, most reported $NiMoO_4$ materials usually show low open space and do not exhibit short diffusion distance, and only the surface part of electroactive materials can be effectively used, which leads to a less satisfactory areal-specific-capacitance (ASC).[35] Therefore, it is urgent to find the way to boost the electrochemical utilization and aggrandize ASC pseudocapacitive materials. A smart and rational concept is to directly grow integrated array architectures with the combination of two types of materials and/or nanostructures on conducting substrates as binder-free electrodes for supercapacitors.[12,26,34-45] So far, there have been some reported works about 3D core/shell structure for supercapacitors. Despite these achievements, choosing novel suitable electrode materials and their assemblies in appropriate architecture to achieve better performance still remains a challenge due to the complicated synthesis processes.

In this work, we chose $NiMoO_4$ NWAs with their high chemical stability as "core" due to the good electron conductivity to provide a direct path for the electrons transport and create channels for the effective transport of electrolyte, chose ultrathin $Co(OH)_2$ nanosheet with high theoretical capacity (3000 F g^{-1}) as "shell" because of the enlarged surface area to shorten ion diffusion path and provide more efficient contacts between the electrolyte ions and active materials for Faradaic energy storage.[36] Therefore, such rational design of $NiMoO_4$@$Co(OH)_2$ core/shell structure with fascinating synergistic properties would provide high ASC capacitance, and the possibility of efficient transport of electrons and ions.

We developed a cost-effective and simple strategy to fabricate $NiMoO_4$@$Co(OH)_2$ core/shell NWAs on Ni foam as a SCs electrode for the first time, with the uniform $NiMoO_4$ nanowires as the "core" via a hydrothermal method and ultrathin $Co(OH)_2$ nanoflakes as the "shell" by electrodeposition.[26-34] The electrode possesses several advantages as follows: (I) $NiMoO_4$ NWAs with high capacitance and stability directly grown on conductive Ni foam serve as both backbone and electron "superhighway" for charge storage and delivery; (II) Both of the core $NiMoO_4$ and shell $Co(OH)_2$ materials are good pseudocapacitive materials with redox reactions in the electrolyte, which contribute to the total energy storage;[35] (III) The $NiMoO_4$@$Co(OH)_2$ NWAs are well separated and strongly supported on Ni foam, avoiding the use of polymer binder/conductive additives which decreases the ohmic polarization. In addition, the Ni foam as substrate with 3D porous structure could provide numerous express electron-transport pathways. More importantly, The micropore of Ni foam could facilitate kinetics ion diffusion and provide more efficient contacts between the electrolyte ions and active materials for Faradaic energy storage;[36-45] (IV) The unique $NiMoO_4$@$Co(OH)_2$ core/shell NWAs can provide additional interfaces, where the ultrathin $Co(OH)_2$ nanoflakes are wrapped on the surface of $NiMoO_4$ nanowires to increase high specific surface area and greatly shorten diffusion distance of electrolytes during the charging/discharging process. In the electrode design, not only "core" and "shell" materials are effectively integrated but also an improvement of electrochemical performance is realized. Especially, compared with pure $NiMoO_4$ NWAs, the $NiMoO_4$@$Co(OH)_2$ core/shell NWAs exhibited larger ASC (2.335 F cm^{-2} at 5 mA cm^{-2}), better rate performance, and more stable cycling ability (83% of its initial capacity retained after 5000 cycles).

2. Experimental Section

2.1 Materials synthesis

All the reagents used arose out of analytical grade and purchased from Tianjin Chemical Reagent Co. without any purification process. The $NiMoO_4$ NWAs were synthesized by a simple hydrothermal method. Prior to the synthesis, the Ni foam substrate (length × diameter × thickness = 3 × 2 × 0.1 cm) was rinsed with ethanol and distilled water for 30 min, respectively.

2.1.1 Preparation of $NiMoO_4$ NWAs on Ni foam

In a typical procedure, $Ni(NO_3)_2{\cdot}6H_2O$ (0.698 g, 2.4 mmol) and $Na_2MoO_4{\cdot}2H_2O$ (0.580 g, 2.4 mmol) were dissolved in 20 mL distilled water, respectively, and $Ni(NO_3)_2$ solution was added to Na_2MoO_4 solution dropwise and stirred for 10 minutes. Then the resulting solution was transferred into Teflon-lined stainless steel autoclave liners, and meanwhile Ni foam substrate was immersed into the reaction solution. The liner was sealed in a stainless steel autoclave and maintained at 150°C for 6 h. After reaction, the autoclave was cooled to room temperature. The samples were collected and washed carefully by distilled water and absolute alcohol for several times. The samples were annealed at 400°C in Ar gas for 1 h. Thus the $NiMoO_4$ NWAs were obtained.

2.1.2 Preparation of $NiMoO_4$@$Co(OH)_2$ core/shell NWAs on Ni foam.

The self-supported $NiMoO_4$ NWAs on Ni foam were used as the scaffold for $Co(OH)_2$ nanoflakes through a simple cathodic electrochemical deposition method. The electrochemical deposition was performed in a standard three-electrode glass cell at 25°C, with $NiMoO_4$ NWAs/Ni foam as the working electrode, saturated calomel electrode (SCE) as the reference electrode, and a Pt foil as the counter-electrode. The electrolyte for electrochemical deposition of $Co(OH)_2$ was obtained by dissolving 1.05 g of $Co(NO_3)_2{\cdot}6H_2O$ into 50 mL of distilled water. The $Co(OH)_2$ nanoflake shell was deposited by cyclic voltammetry (CV) as follows. The CV deposition was conducted in the potential range of −0.5 to −1.1 V with a sweep rate of 10 mV s^{-1} for 4 cycles. The substrate was taken out and rinsed with distilled water and absolute alcohol for several times. The sample was dried overnight at 60°C in a vacuum oven. Finally, the $NiMoO_4$@$Co(OH)_2$ core/shell NWAs were obtained. The mass of active materials was about 1.1mg cm^{-2}.

2.2 Characterization of the $NiMoO_4$ and $NiMoO_4$@$Co(OH)_2$ core/shell NWAs

The crystal structure of the samples was characterized by X-Ray diffraction (XRD, Cu Kα irradiation) with a SIEMENS D5000 X-ray diffractometer. The morphology and microstructure of the synthesized sample were characterized by scanning electron microscopy (SEM, Hitachi S4800 equipped with an EDS) and a transmission electron microscope (TEM; JEOL-2010 with an accelerating voltage of 200 kV).

2.3 Electrochemical measurements of $NiMoO_4$@$Co(OH)_2$ core/shell NWAs

All the electrochemical experiments were performed on a CHI660e electrochemical workstation (Chenhua, Shanghai) containing 2 M KOH aqueous solution as the electrolyte. The NWAs/Ni foam worked as the working electrode, a standard calomel electrode (SCE) was used as the reference electrode, and a Pt foil was used as the counter-electrode. CV measurements were carried out at a scanning rate of 5 to 100 mV s^{-1} between −0.2 and 0.8 V at 25 °C. The specific capacitance is calculated according to the following equation:[38,39]

$$C = \frac{i \times t}{\Delta u} \quad (1)$$

where C is specific capacitance, i represents discharge current density (A cm^{-2} or A g^{-1}), Δu is the potential (V), and t is discharge time (s). Electrochemical impedance spectroscopy (EIS) measurements were made with a superimposed 5 mV sinusoidal voltage in a frequency range from 0.01 Hz to 100 kHz at open circuit potential.

3. Results and discussion

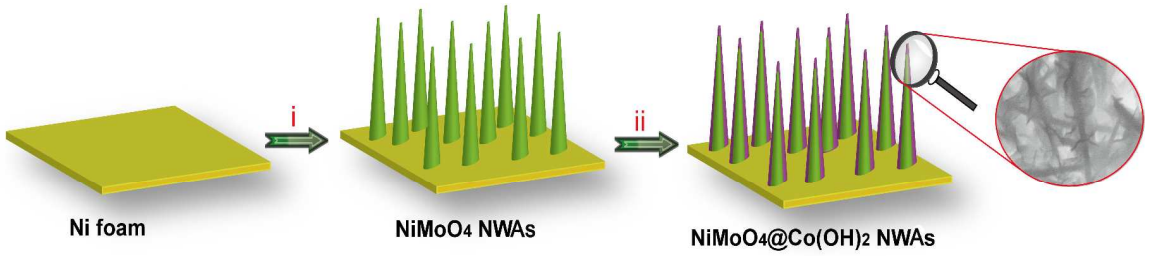

Schematic 1 The representative synthetic procedure and structure details of the $NiMoO_4$@$Co(OH)_2$ core/shell NWAs on Ni foam.

The fabrication of $NiMoO_4$@$Co(OH)_2$ core/shell NWAs directly on Ni foam substrate involves two key steps, as shown in Schematic 1. Firstly, $NiMoO_4$ NWAs are grown on Ni foam substrate via a hydrothermal reaction. Subsequently, $Co(OH)_2$ ultrathin layers are coated on the surface of $NiMoO_4$ NWAs by electrochemical deposition and $NiMoO_4$@$Co(OH)_2$ core/shell nanowire arrays are obtained.

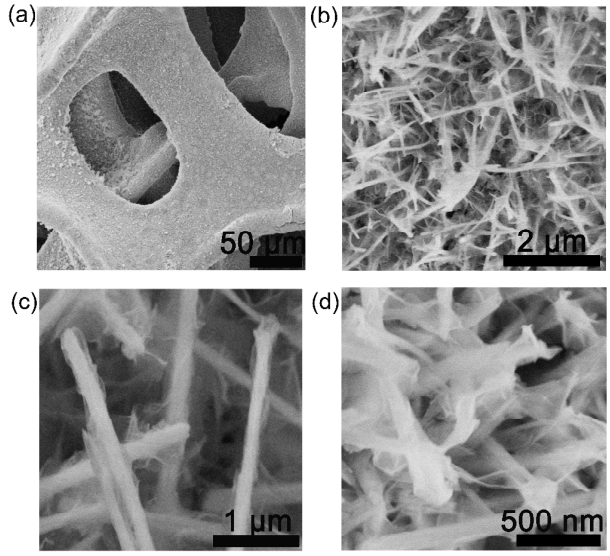

Figure 1 Low-magnification (a) and high-magnification (b,c,d) SEM images of the $NiMoO_4$@$Co(OH)_2$ NWAs on Ni foam.

Morphologies of the $NiMoO_4$ and $NiMoO_4$@$Co(OH)_2$ NWAs were examined by SEM. The $NiMoO_4$ NWAs cover uniformly on the substrate (Figure S1 in the Electronic Supplementary Information, ESI). The low-magnification SEM image in Figure 1a shows the products on the skeletons of the Ni foam, and they are uniformly distributed. Figure 1b,c display that the ultrathin $Co(OH)_2$ nanoflakes are wrapped on the $NiMoO_4$ NWAs. Figure 1d shows these ultrathin nanoflakes with a thickness of about 10 nm to 20 nm connected with each other to form a stable structure. In addition, to investigate the height of the NWA on Ni foam, the cross section SEM image of the $NiMoO_4$@$Co(OH)_2$ NWAs has been shown in Figure S2. Obviously, the height of the NWA is about 2.2 μm.

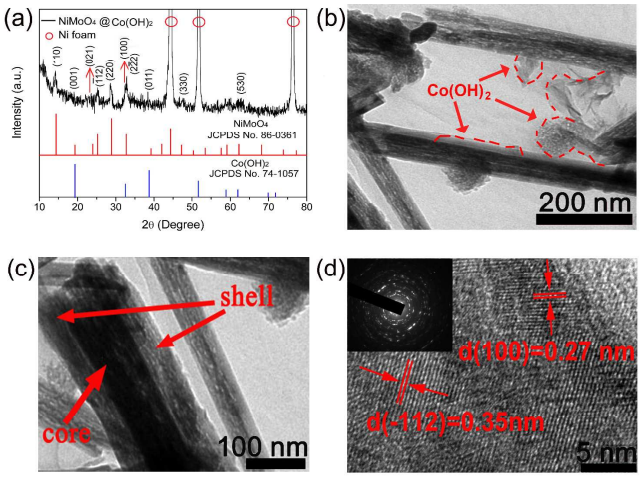

Figure 2 (a) XRD patterns of the $NiMoO_4$@$Co(OH)_2$ NWAs on Ni foam. (b) and (c) TEM images of the $NiMoO_4$@$Co(OH)_2$ NWAs scraped down from Ni foam. (d) HRTEM image of the $NiMoO_4$@$Co(OH)_2$ NWAs, the inset is the SAED pattern.

Figure 2a shows the XRD patterns of the $NiMoO_4$@$Co(OH)_2$ NWAs on Ni foam (XRD patterns for $NiMoO_4$ NWAs are shown in Figure S3). XRD pattern indicates that the diffraction peaks can be indexed to $NiMoO_4$, which agree well with the reported values of JCPDS No. 86-0361. Moreover, the characteristic (100) peak at 32.5° and (011) peak at 38.0° are the typical peak of $Co(OH)_2$ (JCPDS card No.74-1057), indicating the successful formation of $Co(OH)_2$. The energy dispersive X-ray spectroscopy (EDS) analysis, as shown in Figure S4, demonstrates the existence of Co and Mo elements in the obtained material. Transmission electron microscopy (TEM) measurements were carried out to further investigate the structure of the $NiMoO_4$@$Co(OH)_2$ NWAs. Figure 2b and 2c depict

the low-magnification TEM image of the $NiMoO_4$@$Co(OH)_2$ NWAs after a strong ultrasonic vibration in ethanol, which is consistent with the SEM observation. The high-resolution TEM (HRTEM) image in Figure 2d reveals well-resolved lattice planes of the $NiMoO_4$@$Co(OH)_2$ NWAs, and the lattice fringes show an inter planar spacing of 0.35 nm, corresponding to the (-112) crystal planes of $NiMoO_4$. The lattice fringes show an inter planar spacing of 0.27 nm, corresponding to the (100) crystal plane of $Co(OH)_2$. The SAED pattern (inset in Figure 2d) further shows a well-defined lattice, confirming the polycrystalline characteristics.

The electrochemical measurements were performed in a three-electrode configuration with 2 M KOH as the electrolyte. Typical CV curves of the $NiMoO_4$@$Co(OH)_2$ NWAs under various scan rates are shown in Figure 3a. The CV curves of $NiMoO_4$ are also shown Figure S5a. A pair of strong redox peaks can be found in each CV curve, indicating that the capacitance characteristic is mainly governed by Faradaic redox reactions. The two primary redox couples mainly governed by redox mechanism can be expressed as follows:[19,24,28,34]

$$Ni^{2+} \Leftrightarrow Ni^{3+} + e^{-}; \quad (2)$$

$$Co(OH)_2 + OH^{-} \Leftrightarrow CoOOH + H_2O + e^{-}; \quad (3)$$

$$CoOOH + OH^{-} \Leftrightarrow CoO_2 + H_2O + e^{-}. \quad (4)$$

Figure 3b shows the galvanostatic charge/discharge profiles of the $NiMoO_4$@$Co(OH)_2$ NWAs at different current densities ranging from 5 to 50 mA cm^{-2} (Figure S5c for $NiMoO_4$ NWAs). For comparison, the CV curves and charging/discharging voltage profiles of pristine $NiMoO_4$ NWs are also shown in the Supplementary, Figure S5b and 5d. The voltage plateaus can be seen, approximately 0.2 to 0.3 V which matches well with the peaks observed in the CV curve. On the basis of eq (1), the specific capacitances of the $NiMoO_4$@$Co(OH)_2$ NWAs were calculated to be 2.335, 1.820, 1.620, 1.472, 1.215, 1.056 and 0.909 F cm^{-2} (2122.7, 1654.5, 1472.7, 1338.2, 1104.5 and 960, 826.4 F g^{-1}) at current densities of 5, 10, 15, 20, 30, 40 and 50 mA cm^{-2} (4.5, 9.1, 13.6, 18.2, 27.3, 36.4 and 45.4 A g^{-1}), respectively. These results indicated that the $NiMoO_4$@$Co(OH)_2$ NWAs exhibited high capacitance and good rate capability. The areal specific capacitance (C_{sp}) based on the mass of all active materials versus current density plots are also shown in Figure 3c. At 5 mA cm^{-2}, the $NiMoO_4$@$Co(OH)_2$ NWAs can achieve 2.335 F cm^{-2}, and even at a current density of 50 mA cm^{-2}, they can deliver a C_{sp} of 0.909 F cm^{-2}. However, the $NiMoO_4$ NWAs can achieve 1.229 F cm^{-2}, 0.549 F cm^{-2} at current densities of 5 mA cm^{-2} and 50 mA cm^{-2}, respectively. Through figure S5 b and d comparative analysis, the core/shell structure has a better electrochemical performance. This is mainly attributed to the great contribution of ultrathin $Co(OH)_2$ nanoflakes which enhancive electrochemical redox reaction to boost the charge storage capability.[40] In addition, the long-term cycle stability of the $NiMoO_4$ and $NiMoO_4$@$Co(OH)_2$ NWAs were also investigated by repeating the chronopotentiometry (CP) tests at a current density of 20 mA cm^{-2} for 5000 cycles, and the results are presented in Figure 3d. The areal capacitance of $NiMoO_4$@$Co(OH)_2$ NWAs electrode reaches 1.472 F cm^{-2} in the first cycle and it gradually decreases to 1.221 F cm^{-2} after 5000 cycles, resulting in an overall capacitance loss of only 17%. For contrast, the areal capacitance of $NiMoO_4$ NWAs electrode reaches 0.8192 F cm^{-2} in the first cycle and it gradually decreases to 0.6553 F cm^{-2} after 5000 cycles, resulting in an overall capacitance loss of about 20%. Obviously, the $NiMoO_4$@$Co(OH)_2$ NWAs electrode displays higher areal capacitance and better cycling stability than the $NiMoO_4$ NWAs electrode.

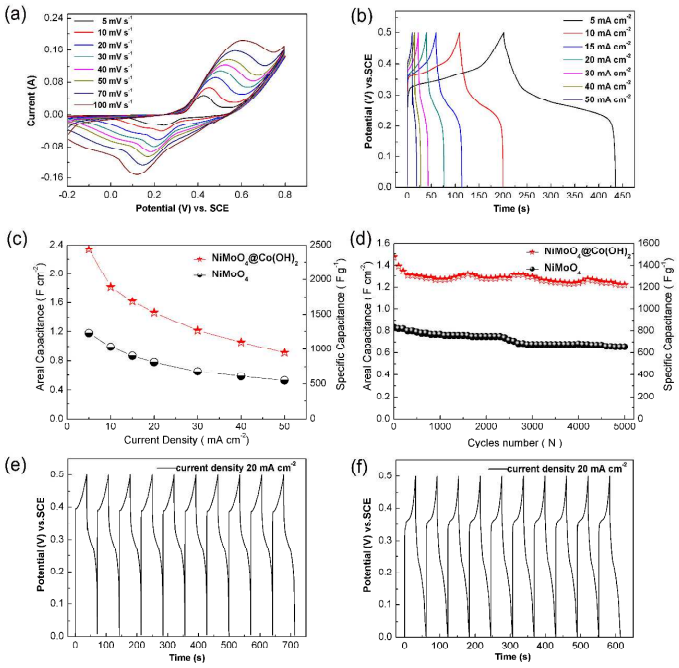

Figure 3 (a) The CV curves of the $NiMoO_4$@$Co(OH)_2$ NWAs electrode at different scan rates. (b) Galvanostatic current charge/discharge curves of the $NiMoO_4$@$Co(OH)_2$ NWAs electrode at different current densities. (c) The areal capacitance and specific capacitance at different current densities. (d) Cycling performance of the $NiMoO_4$@$Co(OH)_2$ and $NiMoO_4$ NWAs electrode. (e), (f) The charge/discharge curves of the first and last 10 cycles, respectively.

Figure 3e and 3f illustrate the first and last ten cycles of representative voltage profiles of the $NiMoO_4$@$Co(OH)_2$ NWAs electrode from galvanostatic charge/discharge measurements. Although, there is attenuation of C_{sp} from the $NiMoO_4$@$Co(OH)_2$ NWAs, the final C_{sp} (1.2208 F cm^{-2}) is still better than that of pure $NiMoO_4$ NWAs (0.8192 F cm^{-2}). The capacitance loss occurred mainly during the first several hundred cycles and then remained stable after this stage. The decay of the capacitance is generally explained by the mechanical arrays' collapse and the dissolution of some electrode material during the cycling.[41,42] The corresponding coulombic efficiencies are obtained from the first cycles to 5000 cycles at 20 mA cm^{-2} during the discharge/charge processes. Most values are over 99% show in Fig S6. Undoubtedly, such good performance of the $NiMoO_4$@$Co(OH)_2$ NWAs can be attributed to the $Co(OH)_2$ decorated on $NiMoO_4$ NWAs, which increases the surface to volume ratio of the electrode. Their high surface areas and open spaces can not only provide more sites for the adsorption of

ions, but also facilitate the fast intercalation and de-intercalation of active species.[43] Multiple valence states of transition metal cobalt have more advantages in redox reaction, and cobalt salts exhibit good electrochemical performance in pseudocapacitors. The capacitance of $NiMoO_4$@$Co(OH)_2$ NWAs electrode is greatly enhanced compared with previously reported values for $NiMoO_4$ and its composites electrode materials, as shown in table S1, such as, $NiMoO_4 \cdot H_2O$ nanoclusters (680 F g^{-1} at 1 A g^{-1}), $CoMoO_4$-$NiMoO_4$ nanobundles (1039 F g^{-1} at 2.5 mA cm^{-2}), Nano β-$NiMoO_4$-$CoMoO_4 \cdot xH_2O$ composites (1472 F g^{-1} at 5 mA cm^{-2}), GO-1D $NiMoO_4 \cdot nH_2O$ nanorods (367 F g^{-1} at 5 A g^{-1}) etc. The result further proves the great advantages of the $NiMoO_4$@$Co(OH)_2$ core/shell NWAs. Another distinguishing feature of micro-meter scale porous Ni foam substrate can improve the pseudocapacitive performance of electrodes,[46,47] loading the electro-active materials on the concave geometry Ni foam substrate are in contrast to the directly generated nanoparticles, nanorods etc, thus suppressing collapse and aggregation of the active materials. The SCs performance of the $NiMoO_4$@$Co(OH)_2$ core/shell NWAs and NiMoO4 NWAs have been summarized by a radar plot in Figure 4, we can comprehensively evaluate the metrics of as-prepared supercapacitor electrodes, including cycle life, internal resistance, capacitance, etc.[38] These results all reveal the better performance of the $NiMoO_4$@$Co(OH)_2$ NWAs electrode.

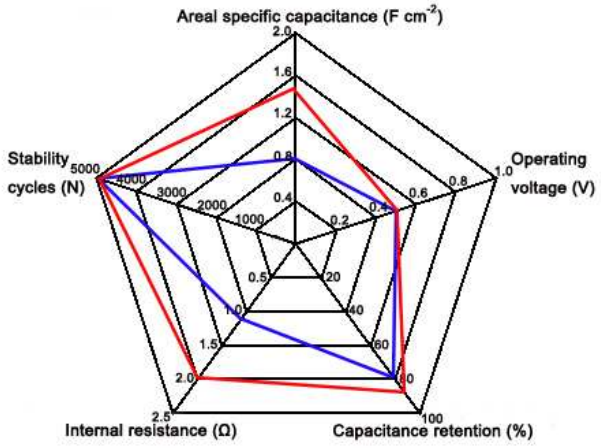

Figure 4 Radar plots to compare the supercapacitor performance of $NiMoO_4$@$Co(OH)_2$ core/shell NWAs (red curves) and NiMoO4 NWAs (blue curves) on Ni foam.

Figure 5 is schematic illustration of electron path about the $NiMoO_4$@$Co(OH)_2$ NWAs on Ni foam, which provides much shorter paths for electron transport and solid structure to improve their capacitive performance. In practice, the $NiMoO_4$@$Co(OH)_2$ NWAs produce more ion migration channels, promote the electrolyte ion transport in three-dimensional space, and not just the edge of the $NiMoO_4$ NWAs. To further investigate the detailed electrochemical characteristics of the supercapacitor electrodes, electrochemical impedance spectroscopy (EIS) measurements were performed in the frequency range of 0.01–100 kHz and the corresponding impedance Nyquist plots are shown in Figure 6, with a well-fitted equivalent circuit showing the components of the whole impedance (R_b is the bulk solution resistance, R_{ct} is the Faradaic interfacial charge-transfer resistance, and W is the Warburg impedance).[43,48] Compared A_1 with B_1, the R_b increased from 1.13 Ω to 2.0 Ω at the high-frequency intercept of the real axis (from the

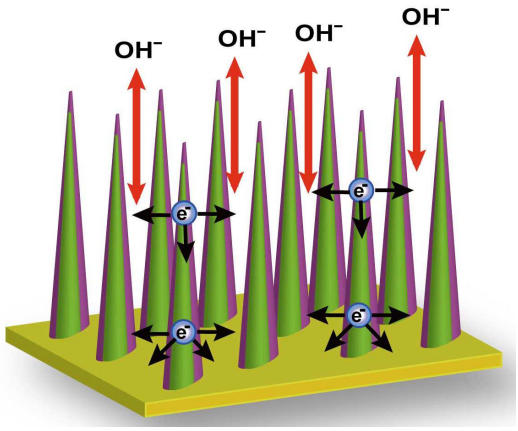

Figure 5 Proposed Schematic illustration of high-performance of the $NiMoO_4$@$Co(OH)_2$ NWAs electrode.

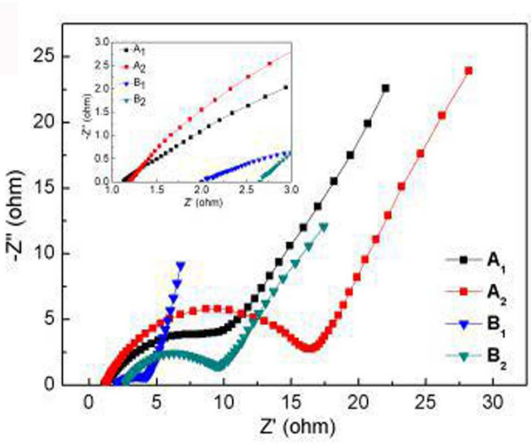

Figure 6 Impedance Nyquist plots of the $NiMoO_4$@$Co(OH)_2$ and $NiMoO_4$ NWAs electrode, the A_1 and A_2 represent the EIS of $NiMoO_4$ NWAs before cycle and after 5000 cycle, respectively; B_1 and B_2 represent EIS of $NiMoO_4$@$Co(OH)_2$ NWAs before cycle and after 5000 cycle, respectively.

inset), suggesting the $NiMoO_4$@$Co(OH)_2$ NWAs electrode shows a bigger R_b than $NiMoO_4$ NWAs electrode. B_1 displays lower charge-transfer resistance and Warburg impedance than A_1. Therefore, the $NiMoO_4$@$Co(OH)_2$ NWAs improve the electron transfer and the occurrence of redox reaction, thereby increasing the capacitance.[43] Compared B_1 with B_2, the internal resistances(R_b) increased from 2.0 Ω to 2.65 Ω at the high-frequency intercept of the real axis after 5000 cycles, which did not change obviously. The Warburg impedance is almost the same after cycle test, indicating the stability of the electrode. The low R_{ct} suggests the large electroactive surface area of the electrode.[48] The large electroactive surface area is owing to the large specific surface area and high electrical conductivity of the ultrathin $Co(OH)_2$ nanoflakes. The slight increase of the R_{ct} after

5000 cycles is probably due to the loss of adhesion of some active material with the current collector, and the corrosion of the current collector caused by the dissolved oxygen in electrolytes during the charge/discharge cycling or matching problems.[49] Compared with $NiMoO_4$ NWAs electrode material, the superior electrochemical performance of the $NiMoO_4$@$Co(OH)_2$ NWAs are mainly attributed to the assembly of ultrathin $Co(OH)_2$ nanoflakes. These interconnected ultrathin nanoflakes have the following advantages: firstly, high conductivity and high specific capacitance are advantageous for fast electron transport; secondly, the ultrathin nanoflakes structure could provide efficient ion and electron transport, giving rise to faster kinetics and resulting in high charge/discharge capacities even at high current densities; Moreover, the ultrathin nanoflakes characteristics of the nanostructure resulted in large surface area, providing more electroactive sites for Faradaic energy storage. On the other side, morphological analysis of the electrodes tested after many cycles could provide worthwhile structural and electrochemical information. As shown in Figure S7 by SEM characterization nanostructures were well maintained with a little structural deformation after 5000 cycles. $Co(OH)_2$ nanoflakes still coated on the surface of the $NiMoO_4$ nanowires with little structural collapse during the oxidation-reduction reaction. $NiMoO_4$@$Co(OH)_2$ NWAs electrode synthesized by electrochemical deposition method is not easily collapsed and fell after thousands of cycles, resulting in a good cycling ability of the arrays. Together with the electrochemical measurements, these results confirm the superiority of our rational design of the $NiMoO_4$@$Co(OH)_2$ core/shell NWAs nanostructure.

4. Conclusions

We have demonstrated a facile and scalable strategy for the direct growth of $NiMoO_4$@$Co(OH)_2$ nanowire arrays on Ni foams via hydrothermal reaction and electrochemical deposition, and the electrochemical properties were investigated. Compared with pure $NiMoO_4$ NWAs, the $NiMoO_4$@$Co(OH)_2$ core/shell NWAs exhibited higher electrical capacity and reliability. Ultrathin $Co(OH)_2$ nanoflakes were assembly on $NiMoO_4$ nanowire arrays, resulting in a high specific surface area, rich accessible electroactive sites, short ion transport pathways, and superior electron collection efficiency. Taking advantages of the synergetic effects, the $NiMoO_4$@$Co(OH)_2$ core/shell NWAs exhibited high ASC, desirable cycle life and rate performance. Our results indicate that the $NiMoO_4$@$Co(OH)_2$ NWAs are promising for high-performance SCs. We believed that our work can contribute to the rational design concept of electrode materials for extensive application.

Acknowledgments

This work was partly supported from the National Natural Science Foundation of China (Grant no. 61376073, 61107023), and the Specialized Research Fund for the Doctoral Program of Higher Education of China (20120161110016, 20110121120020).

Notes and references

[a] Key laboratory for Micro-/Nano-Optoelectronic Devices of Ministry of Education, School of Physics and Electronics, Hunan University, Changsha 410082, China. E-mail address: liqiuhong@xmu.edu.cn.Tel.:86-592-2187198.
[b] Pen-Tung Sah Institute of Micro-Nano Science and Technology of Xiamen University, Xiamen, 361005, China.
[c] Department of Electronic Engineering, School of Information Science and Engineering, Xiamen University, Xiamen 361005, China.

Electronic Supplementary Information (ESI) available: [The XRD patterns and SEM images of $NiMoO_4$ NWs; The cross section image of the $NiMoO_4$@$Co(OH)_2$ NWAs; The EDS patterns of $NiMoO_4$@$Co(OH)_2$ NWAs; CV curves and galvanostatic discharge curves of $NiMoO_4$ NWs and comparison of the $NiMoO_4$@$Co(OH)_2$ and $NiMoO_4$ NWAs electrode; Coulombic efficiency of the $NiMoO_4$@$Co(OH)_2$ NWAs electrode].

1 P. Simon, Y. Gogotsi, *Nat. Mater,* 2008, **7**, 845.
2 Y. Wang, Z. Hong, M. Wei, Y. Xia, *Adv. Funct. Mater,* 2012, **22**, 5185.
3 A. Arico, P. Bruce, B. Scrosati, J. Tarascon, W. Schalkwijk, *Nat. Mater,* 2005, **4**, 366.
4 G. Zhang, H. Wu, H. Hoster, M. Chan–Park, X. Lou, *Energy Environ. Sci,* 2012, **5**, 9453.
5 X. Lu, T. Zhai, X. Zhang, Y. Shen, L.Yuan, B. Hu, L. Gong, J. Chen, Y. Gao, J. Zhou, Y. Tong, Z. Wang, *Adv. Mater,* 2012, **24**, 938.
6 X. Xia, J. Tu, Y. Zhang, X. Wang, C. Gu, X. Zhao, H. Fan, *ACS Nano,* 2012, **6**, 5531.
7 J. Liu, J. Jiang, C. Cheng, H. Li, J. Zhang, H. Gong, H. Fan, *Adv. Mater,* 2011, **23**, 2076.
8 J. Liu, J. Jiang, M. Bosmanc, H. Fan, *J. Mater. Chem,* 2012, **22**, 2419.
9 H. Jiang, C. Li, T. Sun, J. Ma, *Chem. Commun,* 2012, **48**, 2606.
10 G. Li, Z. Wang, F. Zheng, Y. Ou, Y. Tong, *J. Mater. Chem,* 2011, **21**, 4217.
11 J. Kim, K. Zhu, Y. Yan, C. Perkins, A. Frank, *Nano Lett,* 2010, **10**, 4099.
12 Q. Yang, Z. Lu, T. Li, X. Sun, J. Liu, *Nano Energy*, 2014, **7**, 170.
13 L. Mai, F. Yang, Y. Zhao, X. Xu, L. Xu, Y. Luo, *Nat. Commun,* 2011, **2**, 2041.
14 J. Yan, E. Khoo, A. Sumboja, P. Lee, *ACS Nano,* 2010, **4**, 4247.
15 L. Bao, J. Zang, X. Li, *Nano Lett,* 2011, **11**, 1215.
16 D. Cai, D. Wang, B. Liu, Y. Wang, Y. Liu, L. Wang, H. Li, H. Huang, Q. Li, T. Wang, *ACS Appl. Mater,* 2013, **5**, 12905.
17 M. Liu, L. Kong, C. Lu, X. Ma, X. Li, Y. Luo, L. Kang, *J. Mater. Chem. A,* 2013, **1**, 1380.
18 B. Senthilkumar, D. Meyrick, Y. Lee, R. Selvan, *RSC Adv,* 2013, **3**, 16542.
19 M. Liu, L. Kang, L. Kong, C. Lu, X. Ma, X. Li, Y. Luo, *RSC Adv,* 2013, **3**, 6472.
20 B. Senthilkumar, K. Sankar, R. Selvan, M. Danielle, M. Manickam, *RSC Adv,* 2013, **3**, 352.
21 D. Cai, B. Liu, D. Wang, Y. Liu, L. Wang, H. Li, Y. Wang, C. Wang, Q. Li, T. Wang, *Electrochimica Acta,* 2014, **115**, 358.
22 H. Wan, J. Jiang, X. Ji, L. Miao, L. Zhang, K. Xu, H. Chen, Y. Ruan, *Mater.Lett,* 2013, **108**, 164.
23 D. Ghosh, S. Giri, C. Das, *Nanoscale,* 2013, **5**, 10428.
24 D. Guo, P. Zhang, H. Zhang, X. Yu, J. Zhu, Q. Li, T. Wang, *J. Mater. Chem. A,* 2013, **1**, 9024.

25 D. Cai, B. Liu, D. Wang, Y. Liu, L. Wang, H. Li, Y. Wang, C. Wang, Q. Li, T. Wang, *Electrochimica Acta,* 2014, **125**, 294.
26 X. Xia, J. Tu, Y. Zhang, J. Chen, X. Wang, C. Gu, C. Guan, J. Luo, H. Fan, *Chem. Mater,* 2012, **24**, 3793.
27 J. Chang, C. Wu, I. Sun, *J. Mater. Chem,* 2010, **20**, 3729.
28 L. Kong, M. Liu, J. Lang, M. Liu, Y. Luo, L. Kang, *J Solid State Electrochem,* 2011, **15**, 571.
29 Z. Yu, Y. Dai, W. Chen, *J. Chin. Chem. Soc,* 2010, **57**, 423.
30 W. Zhou, D. Zhao, M. Xu, H. Li, *Electrochimica Acta,* 2008, **53**, 7210.
31 A. Jagadale, V. Kumbhar, D. Dhawale, C. Lokhande, *Electrochimica Acta,* 2013, **98**, 32.
32 S. Kandalkar, H. Lee, H. Chae, C. Kim, *Mater. Res. Bull,* 2011, **46**, 48.
33 V. Gupta, T. Kusahara, H. Toyama, S. Gupta, N. Miura, *Electrochem. Commun,* 2007, **9**, 2315.
34 L. Huang, D. Chen, Y. Ding, S. Feng, Z. Wang, M. Liu, *Nano Lett,* 2013, **13**, 3135.
35 L.Yu, G. Zhang, C.Yuan, X. Lou, *Chem. Commun,* 2013, **49**, 137.
36 C. Zhou, Y. Zhang, Y. Li, J. Liu, *Nano Lett,* 2013, **13**, 2078.
37 H. Chen, L. Hu, Y. Yan, R. Che, M. Chen, L. Wu, *Adv. Energy Mater,* 2013, **3**, 1636.
38 G. Xiong, C. Meng, R. Reifenberger, P. Irazoqui, T. Fisher, *Electroanalysis*, 2014, **26**, 30.
39 G. Yu, L. Hu, M. Vosgueritchian, H. Wang, X. Xie, J. McDonough, X. Cui, Y. Cui, Z. Bao, *Nano Lett*. 2011, **11**, 2905.
40 G. Zhang, T. Wang, X.Yu, H. Zhang, H. Duan, B. Lu, *Nano Energy,* 2013, **2**, 586.
41 L. Mei, T. Yang, C. Xu, M. Zhang, L. Chen, Q. Li, T. Wang, *Nano Energy,* 2014, **3**, 36.
42 J. Jiang, Y. Li, J. Liu, X. Huang, C. Yuan, X. Lou, *Adv. Mater,* 2012, **24**, 5166.
43 H. Zhang, Y. Chen, W. Wang, G. Zhang, M. Zhuo, H. Zhang, T.Yang, Q. Li, T. Wang, *J. Mater. Chem. A,* 2013, **1**, 8593.
44 G. Xiong, C. Meng, R. Reifenberger, P. Irazoqui, T. Fisher, *Adv. Energy Mater,* 2014, **4**, 1300515.
45 G. Xiong, K. Hembram, R. Reifenberger, T. Fisher. *Journal of Power Sources,* 2013, **227**, 254.
46 G.Yang, C. Xu, H. Li, *Chem. Commun,* 2008, 6537.
47 W. Zhou, M. Xu, D. Zhao, C. Xu, H. Li, *Microporous Mesoporous Mater,* 2009, **117**, 55.
48 M. Wu, H. Hsieh, *Electrochimica Acta,* 2008, **5**, 3427.
49 Z. Fan, J. Yan, T. Wei, L. Zhi, G. Ning, T. Li, F. Wei, *Adv. Funct. Mater,* 2011, **21**, 2366.